2026 American Control Conference (ACC)
May 27-29, 2026. New Orleans, Louisiana, USA

Dense Extended Kalman Filter for Simultaneous Cell State-Parameter Estimation

Luke Nuculaj and Jun Chen*, *Senior Member, IEEE*

***Abstract*— This work investigates the use of dense extended Kalman filter (DEKF) to simultaneously estimate both the state-of-charge (SOC) and equivalent-circuit parameters of serial-connected, lithium-ion battery cells under limited voltage measurement. Stability analyses are conducted to certify the reliability of the DEKF for simultaneous state-parameter estimation under certain mild assumptions. To begin, the local asymptotic stability of the expected dense error in the presence of nonlinearity is verified by selection of an appropriate Lyapunov function. Then the expected sparse error is shown to be marginally stable in the absence of nonlinearities by proving that the spectral radius of the sparse expected error dynamics is exactly equal to 1. Finally, a sufficient condition for sparse stability in the presence of nonlinearity is obtained via selection of an appropriate Lyapunov function. Simulation trials under several different scenarios are executed, confirming that the associated error dynamics are indeed stable for the duration of the simulation time.**

I. Introduction

In recent years, electric vehicles (EVs) have emerged as a commercially-dominant technology to mitigate global carbon emissions. EVs source their electrical energy from interconnected networks of battery cells, typically lithium-ion (Li-Ion), contained within a single battery pack. However, inherent manufacturing variations give rise to cell-to-cell inconsistencies. Specifically, some cells may expend energy more rapidly than others, directly inhibiting range extension since any series-arrangement of cells is only as efficient as its weakest member. One popular mitigation strategy is active cell balancing, which moves charge from stronger cells to weaker ones [1]. Precise balancing control requires knowledge of each cell's state-of-charge (SOC), an intangible quantity that cannot be directly measured and must instead be estimated in real-time. Model-based estimation methods are popular in literature [2], with the extended Kalman filter (EKF) widely studied for its consideration of process and measurement noise. However, simultaneous SOC estimation over many cells poses significant computational challenges [3], and reliable estimation requires accurate knowledge of cell parameters (resistances and capacitances) that evolve with age. Since these parameters also inform state-of-health (SOH) and remaining service life [2], they too must be estimated.

To address these concerns, this paper contributes by first extending the DEKF algorithm to account for parameter estimation by way of artificial perturbations inserted into the system dynamics. Following this, proofs of stability for the dense and sparse error produced by the modified DEKF estimation are presented under mild assumptions. The proof of dense error stability establishes a candidate Lyapunov function, which is instrumental in proving local asymptotic stability of the dense error dynamics. Sparse error stability is proven by demonstrating the spectral radius of the sparse error dynamics to be equal to 1. Afterwards, a sufficient condition for the asymptotic stability of the sparse error is presented in the case of a nonlinear measurement function, which aligns more closely with practical scenarios. Finally, to validate the theoretical findings, experimental simulations are conducted to confirm the efficacy of DEKF for simultaneous SOC and parameter estimation, where three heterogeneous cells are connected in series and subjected to a constant load current. The SOCs and parameters of each cell are estimated under two scenarios: guaranteed stability and increased noise with loss of stability guarantee. In all cases, the average RMSE of the estimates is shown to stabilize within $\leq 1\%$ of the true values after $\leq 35\%$ of the total simulation time has elapsed. Furthermore, the spectral radius of the sparse and dense error dynamics in each case are analyzed to demonstrate the stability.

II. Notation

Let $\mathbb{R}$, $\mathbb{R}^n$, $\mathbb{R}^{m\times n}$, and $\mathbb{Z}$ denote the field of real numbers, the set of real column vectors of length n, the set of m-by-n real matrices, and the set of integers, respectively. The transpose of a matrix $A \in \mathbb{R}^{m\times n}$ is denoted by $A^\top$. The null matrix (0_n) and identity matrix (I_n) are written with a subscript indicating their size. The Moore-Penrose pseudoinverse of A is $A^\dagger := (A^\top A)^{-1}A^\top$. The spectrum of $M \in \mathbb{R}^{m\times m}$ is $\Lambda(M) := \{\lambda \in \mathbb{C} : \det(M - \lambda I) = 0\}$ with spectral radius $\rho(M) := \max\{|\lambda| : \lambda \in \Lambda(M)\}$. The matrix inequality $\alpha_1 I \leq A \leq \alpha_2 I$ means all eigenvalues of A lie in $\mathbb{R}_{[\alpha_1,\alpha_2]}$. $\|\cdot\|$ denotes the Euclidean norm for vectors and induced Euclidean norm for matrices. The Minkowski sum is $A \oplus B := \{a + b : a \in A, b \in B\}$, and $\{\cdot\}^n$ denotes a set with n repeated elements. The superscript $(\cdot)^i$ denotes the ith cell in an N-cell pack ($N \in \mathbb{Z}_{>0}$), and the subscript $(\cdot)_k$ the time step k ($k \in \mathbb{Z}_{\geq 0}$). Subscript $(\cdot)_\mu$ refers to DEKF variables of dimension $n_\mu \in \mathbb{Z}_{>0}$. A circumflex $\hat{x}$ indicates an estimate, with $\hat{x}_{k+1|k}$ and $\hat{x}_{k+1|k+1}$ the prior and posterior estimates, respectively. Subscripts and superscripts combine naturally (e.g., $\hat{x}^i_{k|k-1}$ is the prior estimate of cell i at time k).

This work is supported in part by the National Science Foundation through Awards #2237317 and #2430374. *Corresponding author: J. Chen.* The authors are with the Department of Electrical and Computer Engineering, Oakland University, Rochester, MI 48309, USA (email: {lukenuculaj, junchen}@oakland.edu).

III. Cell State and Parameter Estimation

A. Battery Model

We consider an N-cell serial-connected string, where each cell's highly nonlinear dynamics are approximated with an ECM [4], [5]. For this specific cell model, we have the following discrete-time dynamics

$$s_{k+1}^i = s_k^i - \eta^i \frac{T_s}{3600C^i} u_k^i, \tag{1a}$$
$$V_{k+1}^i = \left(1 - \frac{T_s}{R_p^i C_p^i}\right) V_k^i + \frac{T_s}{C_p^i} u_k^i, \tag{1b}$$
$$y_k^i = V_{oc,k}^i - V_k^i - R_o^i u_k^i, \tag{1c}$$

where T_s is the sampling period in seconds, s^i is the ith cell's SOC, V^i is the relaxation voltage, V_{oc}^i is the open-circuit voltage (OCV), R_o^i is the open-circuit resistance, R_p^i is the relaxation resistance, C_p^i is the relaxation capacitance, η^i is the Coulombic efficiency, and C^i is the cell capacity with unit of Amp-hours. Furthermore, y^i is the terminal voltage, and u^i denotes the net cell current, which is the sum of the balancing current β^i and the load current u. Lastly, $u^i > 0$ signifies discharging and $u^i < 0$ charging of the cell.

Defining the state vector $x_k^i := \begin{bmatrix} s_k^i & V_k^i \end{bmatrix}^\top$, (1a) and (1b) can be combined to yield the dynamic equation $x_{k+1}^i = A^i x_k^i + B^i u_k^i$, where $A^i := \operatorname{diag}\left\{1, 1 - \frac{T_s}{R_p^i C_p^i}\right\} \in \mathbb{R}^{2\times 2}$, and $B^i := \begin{bmatrix} -\eta^i \frac{T_s}{3600C^i} & \frac{T_s}{C_p^i} \end{bmatrix}^\top \in \mathbb{R}^{2\times 1}$. However, real-life systems do not adhere exactly to mathematical models, so the dynamic equation and (1c) are more accurately represented as

$$x_{k+1}^i = A^i x_k^i + B^i u_k^i + w_k^i, \tag{2a}$$
$$y_{k+1}^i = V_{oc,k}^i - V_k^i - R_o^i u_k^i + v_k^i, \tag{2b}$$

where process noise $w_k^i \sim \mathcal{N}(0, Q_k^i) \in \mathbb{R}^2$ and measurement noise $v_k^i \sim \mathcal{N}(0, R_k^i) \in \mathbb{R}$ are assumed to be follow zero-mean Gaussian distributions with covariance matrices $Q_k^i \in \mathbb{R}^{2\times 2} \succeq 0$ and $R_k^i \in \mathbb{R}_{>0}$. To model series-connected cells with single pack terminal voltage measurement, (2) can be extended to produce the following

$$x_{k+1} = Ax_k + Bu_k + w_k, \tag{3a}$$
$$y_k = \sum_{i=1}^{N} \left(V_{oc,k}^i - V_k^i - R_o^i u_k^i\right) + v_k, \tag{3b}$$

where $A = \operatorname{blkdiag}\{A^i\}_{i=1}^N \in \mathbb{R}^{2N\times 2N}$, $B = \operatorname{blkdiag}\{B^i\}_{i=1}^N \in \mathbb{R}^{2N\times N}$, $x_k \in \mathbb{R}^{2N}$, $u_k \in \mathbb{R}^N$, $w_k := \begin{bmatrix} w_k^1 & w_k^2 & \dots & w_k^N \end{bmatrix}^\top \in \mathbb{R}^{2N}$, $v_k := \sum_{i=1}^N v_k^i \sim \mathcal{N}(0, N^2 R_k^i)$.

Conventionally, the EKF algorithm as applied to the SOC estimation for battery packs with limited measurement uses the mathematical model (3a) in the time update

$$\hat{x}_{k+1|k} = A\hat{x}_{k|k} + Bu_k, \tag{4a}$$
$$P_{k+1|k} = AP_{k|k}A^\top + Q_k, \tag{4b}$$

and corrects this prediction with the terminal voltage measurement y_k in the measurement update

$$L_{k+1} = \frac{P_{k+1|k} H_{k+1}^\top}{H_{k+1} P_{k+1|k} H_{k+1}^\top + R_k}, \tag{5a}$$
$$\hat{x}_{k+1|k+1} = \hat{x}_{k+1|k} + L_{k+1}\left(y_{k+1} - h(\hat{x}_{k+1|k}, u_k)\right), \tag{5b}$$
$$P_{k+1|k+1} = (I_N - L_{k+1}H_{k+1})P_{k+1|k}, \tag{5c}$$

where $P_{k+1|k}, P_{k+1|k+1} \in \mathbb{R}^{2N\times 2N}$ are the predicted and updated process covariance matrices, process noise covariance $Q_k := \operatorname{blkdiag}\{Q_k^i\}_{i=1}^N \in \mathbb{R}^{2N\times 2N}$, measurement noise covariance $R_k := N^2 R_k^i$, Kalman gain $L_k \in \mathbb{R}^{2N}$, measurement function $h(\hat{x}_{k+1|k}, u_k) : \mathbb{R}^{2N\times N} \mapsto \mathbb{R} := \sum_{i=1}^N \left(V_{oc,k}^i - V_k^i - R_o^i u_k^i\right)$, and observation matrix $H_{k+1} := \left.\frac{\partial h}{\partial x}\right|_{x=\hat{x}_{k+1|k}} = \begin{bmatrix} \left.\frac{\partial V_{oc}^1}{\partial s^1}\right|_{s=\hat{s}_{k+1|k}^1} & -1 & \cdots & \left.\frac{\partial V_{oc}^N}{\partial s^N}\right|_{s=\hat{s}_{k+1|k}^N} & -1 \end{bmatrix} \in \mathbb{R}^{1\times 2N}$.

B. Dense Extended Kalman Filter

While the EKF is a reliable estimation solution, the amount of computation in (4) and (5) scales in proportion to N^3 by fault of matrix multiplications involving $2N$-by-$2N$ matrices, making real-time implementation of the EKF nonviable in this case. As an alternative, the DEKF proposed in [6] aims to address this issue. This section briefly reviews DEKF and readers are referred to [6] for more details.

DEKF uses the forcing terms in the time update to assign an RFF to each cell as follows

$$\hat{\gamma}_{s,k}^i := \frac{\frac{\eta^i}{C^i} u_k^i}{\frac{1}{N}\sum_{i=1}^N \frac{\eta^i}{C^i} u_k^i}, \quad \hat{\gamma}_{V,k}^i := \frac{\frac{u_k^i}{C_p^i} - \frac{\hat{V}_{k|k}^i}{\tau_p^i}}{\frac{1}{N}\sum_{i=1}^N \left(\frac{u_k^i}{C_p^i} - \frac{\hat{V}_{k|k}^i}{\tau_p^i}\right)}. \tag{6}$$

Each cell has an RFF $\hat{\gamma}_{s,k}^i$ for its SOC and another RFF $\hat{\gamma}_{V,k}^i$ for its relaxation voltage, where $\hat{\gamma}_{s,k}^i, \hat{\gamma}_{V,k}^i \in \mathbb{R}$ for all $i \in \mathbb{Z}_{[1,N]}$ and $k \in \mathbb{Z}_{\geq 0}$. Following this, the RFFs in (6) are first used to construct the cell-level RFF matrix $\hat{\Gamma}_k^i = \left.\frac{\partial x_k^i}{\partial x_{\mu,k}}\right|_{x_k^i=\hat{x}_k^i} := \operatorname{diag}\{\hat{\gamma}_{s,k}^i, \hat{\gamma}_{V,k}^i\} \in \mathbb{R}^{2\times 2}$, which are then combined to obtain the RFF matrix $\hat{\Gamma}_k = \left.\frac{\partial x_k}{\partial x_{\mu,k}}\right|_{x_k=\hat{x}_k} := [\hat{\Gamma}_k^1, \hat{\Gamma}_k^2, \dots, \hat{\Gamma}_k^N]^\top \in \mathbb{R}^{2N\times 2}$. Suppose there exists a reduced-dimensional vector $x_\mu \in \mathbb{R}^2$ which represents the average state over all cells. Then, the RFF matrix provides a means of tracking each cell's state via changes in $x_{\mu,k}$ by computing $x_{k+1} = x_k + \Gamma_k(x_{\mu,k+1} - x_{\mu,k})$. Thus, the initial task of estimating all states in the sparse system (3) is reduced to estimating a dense "average" state and propagating its changes to running sparse estimates via the RFF matrix. Such an undertaking necessitates an appropriate model, which is accomplished by reimagining (3) with the following dense model

$$x_{\mu,k+1} = A_{\mu,k+1}x_{\mu,k} + B_{\mu,k+1}u_k + w_{\mu,k}, \tag{7a}$$
$$y_{\mu,k} = h_\mu(x_k, u_k) + v_{\mu,k}, \tag{7b}$$

where $x_{\mu,k} := \begin{bmatrix} s_{\mu,k} & V_{\mu,k} \end{bmatrix}^\top$, $A_{\mu,k+1} = \hat{\Gamma}_k^\dagger A_{k+1} \hat{\Gamma}_k \in \mathbb{R}^{2\times 2}$, $B_{\mu,k+1} = \hat{\Gamma}_k^\dagger B_{k+1} \in \mathbb{R}^{2\times N}$, $h_\mu(x_k, u_k) = \frac{1}{N} h(x_k, u_k)$, $w_{\mu,k} \sim \mathcal{N}(0, \hat{\Gamma}_k^\dagger Q_k \hat{\Gamma}_k)$ and $v_{\mu,k} \sim \mathcal{N}(0, \frac{1}{N^2} R_k)$. Over this dense model, the DEKF performs the estimation and is able to extrapolate successive differences in the dense state to each sparse state with the propagation step $x_{k+1} = x_k + \Gamma_k(x_{\mu,k+1} - x_{\mu,k})$. For the full listing of the DEKF algorithm, see Algorithm 1. The DEKF's main advantage is reduced computation, since state and covariance matrix dimensions remain constant regardless of cell count, reducing SOC estimation from cubic to linear time complexity. For a complete derivation and floating-point operations analysis, see Sections VI-A, VI-B, and VII-B in [6].

C. Artificial Perturbation for Parameter Estimation

A common solution in the literature to address online parameter estimation is to append the parameters of interest to the state vector and modify the model dynamics A^i and B^i to reflect that their values do not change [7]. Specifically, for open-circuit resistance R_o, the extension yields the new system dynamics matrices $A^i := \operatorname{diag}\left\{1, 1 - \frac{T_s}{R_p^i C_p^i}, 1\right\} \in \mathbb{R}^{3\times 3}$ and $B^i := \begin{bmatrix} -\eta^i \frac{T_s}{3600 C^i} & \frac{T_s}{C_p^i} & 0 \end{bmatrix}^\top \in \mathbb{R}^{3\times 1}$, where the modified cell level state vector becomes $x_k^i = \begin{bmatrix} s_k^i & V_k^i & R_{o,k}^i \end{bmatrix}^\top$. From here, the same block-diagonal constructions for (3) can be repeated to create a pack level model whereby EKF can be used to estimate SOC and R_o^i simultaneously for all $i \in \mathbb{Z}_{[1,N]}$.

Direct parameter embedding in EKF estimation is powerful but problematic when transferred to the DEKF. Without forcing terms in parameter dynamics, RFF computation (6) becomes impossible as both dividend and divisor equal zero. To address this, we propose the direct inclusion of artificial perturbations in the time update: $\hat{x}_{k+1|k}^i = (A_{k+1}^i - \Delta^i)\hat{x}_{k|k}^i + B_{k+1}^i u_k$, where perturbation $\Delta^i := \operatorname{diag}\{0, 0, \delta^i\} \in \mathbb{R}^{3\times 3}$ with $\delta^i \in \mathbb{R}_{>0}$ for all $i \in \mathbb{Z}_{[1,N]}$. From here, if we elect the dense parameter state $R_{o,\mu}$, then the corresponding RFF computation is $\hat{\gamma}_{R_o,k}^i = \delta^i \hat{R}_{o,k|k}^i / \left(\frac{1}{N}\sum_{i=1}^N \delta^i \hat{R}_{o,k|k}^i\right)$, and consequently, the modified RFF matrix $\hat{\Gamma}_k = \begin{bmatrix} \hat{\Gamma}_k^1 & \hat{\Gamma}_k^2 & \dots & \hat{\Gamma}_k^N \end{bmatrix}^\top \in \mathbb{R}^{3N\times 3}$ has its constituent blocks $\hat{\Gamma}_k^i = \operatorname{diag}\{\hat{\gamma}_{s,k}^i, \hat{\gamma}_{V,k}^i, \hat{\gamma}_{R_o,k}^i\} \in \mathbb{R}^{3\times 3}$. Henceforth, we will denote the number of sparse states by $n_\mu N$.

From here, we redefine the terms associated with the original dense model (7) to accommodate parameter estimation as follows:

$$x_{\mu,k} := \begin{bmatrix} s_{\mu,k} & V_{\mu,k} & R_{o,\mu,k} \end{bmatrix}^\top \in \mathbb{R}^{n_\mu}, \tag{8a}$$

$$A_{\mu,k+1} := \hat{\Gamma}_k^\dagger \left(\operatorname{blkdiag}\{A_{k+1}^i - \Delta^i\}_{i=1}^N\right) \hat{\Gamma}_k \in \mathbb{R}^{n_\mu \times n_\mu}, \tag{8b}$$

$$B_{\mu,k+1} := \hat{\Gamma}_k^\dagger (\operatorname{blkdiag}\{B_{k+1}^i\}_{i=1}^N) \in \mathbb{R}^{n_u \times N}, \tag{8c}$$

and the dimension of the sparse process noise covariance $Q_k \in \mathbb{R}^{n_\mu N \times n_\mu N}$ is adjusted accordingly. Algorithm 1 summarize the time update and measurement update of the

Algorithm 1 Perturbed DEKF: Time Update

procedure TIME($\hat{x}_{\mu,k|k}$, $P_{\mu,k}^+$, u_k, $\hat{x}_{k|k}$, Δ)
- $\hat{\Gamma}_k, \hat{\Gamma}_k^\dagger \leftarrow$ compute (6), $\hat{\gamma}_{R_o,k}^i$ for all $i \in \mathbb{Z}_{[1,N]}$;
- $A_{\mu,k+1} \leftarrow$ (8b); $B_{\mu,k+1} \leftarrow$ (8c);
- $\hat{x}_{\mu,k+1|k} \leftarrow A_{\mu,k}\hat{x}_{\mu,k|k} + B_{\mu,k}u_k$;
- $\hat{x}_{k+1|k} \leftarrow \hat{x}_{k|k} + \hat{\Gamma}_k(\hat{x}_{\mu,k+1|k} - \hat{x}_{\mu,k|k})$;
- $P_{\mu,k+1|k} \leftarrow A_{\mu,k+1} P_{\mu,k|k} A_{\mu,k+1}^\top + Q_\mu$;
- $H_{\mu,k+1} \leftarrow$ evaluate $\left.\frac{\partial h}{\partial x}\right|_{x=\hat{x}_{k+1|k}}$;
- $K_{\mu,k+1} \leftarrow P_{\mu,k+1|k} H_{\mu,k+1}^\top \times \left(H_{\mu,k+1} P_{\mu,k+1|k} H_{\mu,k+1}^\top R_{\mu,k+1}\right)^{-1}$;
- $\hat{x}_{\mu,k+1|k+1} \leftarrow \hat{x}_{\mu,k+1|k} + K_{\mu,k+1}(y_{\mu,k+1} - h_{\mu,k+1})$;
- $\hat{x}_{k+1|k+1} \leftarrow \hat{x}_{k+1|k} + \hat{\Gamma}_k(\hat{x}_{\mu,k+1|k+1} - \hat{x}_{\mu,k+1|k})$;
- $P_{\mu,k+1|k+1} \leftarrow (I_{n_\mu} - K_{\mu,k+1} H_{\mu,k+1}) P_{\mu,k+1|k}$
- $k \leftarrow k + 1$

return $\hat{x}_{\mu,k+1|k+1}, P_{\mu,k+1|k+1}, \hat{x}_{k+1|k+1}$

end procedure

perturbed DEKF for simultaneous state-parameter estimation.

D. Stability Analysis Problem Formulation

The stability analysis of any discrete-time estimation algorithm is based primarily on how the error evolves over time. To this end, we define the dense error $\zeta_{\mu,k+1|k} := \hat{x}_{\mu,k+1|k} - x_{\mu,k+1} \in \mathbb{R}^{n_\mu}$, the expected dense error $z_{\mu,k+1|k} := \mathbb{E}\left[\zeta_{\mu,k+1|k}\right]$, the sparse error $\zeta_{k+1|k} := \hat{x}_{k+1|k} - x_{k+1} \in \mathbb{R}^{n_\mu N}$, the expected sparse error $z_{k+1|k} := \mathbb{E}\left[\zeta_{k+1|k}\right]$, and formulate the central problem of this paper as follows.

Problem 1: Consider the dense model (8) for simultaneous state and parameter estimation via artificial perturbations Δ. Using Algorithm 1 to estimate the SOC and open-circuit resistance for each cell, determine whether the sequences $\{z_{\mu,k+1|k}\}_{k=0}^\infty$ and $\{z_{k+1|k}\}_{k=0}^\infty$ are stable, and if so, to what extent.

IV. Stability Analysis

This section introduces standard assumptions for the battery pack characteristics and joint DEKF, which are instrumental for the following proofs.

Assumption 1: $A_{\mu,k}$ is nonsingular for all $k \in \mathbb{Z}_{\geq 0}$.

Assumption 2: The measurement function h is L-smooth over $\mathbb{R}^{n_\mu N}$ with smoothness parameter L, i.e., $\left\|\nabla_x h(x_{k+1}, u_k) - \nabla_x h(\hat{x}_{k+1|k}, u_k)\right\| \leq L\left\|x_{k+1} - \hat{x}_{k+1|k}\right\|$ for all $x_{k+1|k}, \hat{x}_{k+1|k} \in \mathbb{R}^{n_\mu N}$.

We define the nonlinearity of the measurement function as $\chi(x_{k+1}, \hat{x}_{k+1|k}, u_k) := h(x_{k+1}, u_k) - h(\hat{x}_{k+1|k}, u_k) - H_{k+1}(x_{k+1} - \hat{x}_{k+1|k})$, and we may apply Taylor's theorem to obtain the known upper bound $\|\chi(x_{k+1}, \hat{x}_{k+1}, u_k)\| \leq \frac{L}{2}\|x_{k+1} - \hat{x}_{k+1}\|^2$ on L-smooth functions.

Assumption 3: $\left\|\hat{\Gamma}_{k+1} - \hat{\Gamma}_k\right\| = 0$ for all $k \in \mathbb{Z}_{\geq 0}$.

Assumption 3 requires time invariance of $\hat{\Gamma}_k$ (i.e., $\hat{\Gamma}_i = \hat{\Gamma}_j$ for all $i, j \in \mathbb{Z}_{\geq 0}$). While restrictive in some cases, this assumption is useful when balancing currents are absent, as it eliminates repeated recomputation of $\hat{\Gamma}_k$ once relaxation voltage estimates stabilize.

A. Dense Stability Analysis

This section investigates the first half of Problem 1, which is devoted to determining the asymptotic behavior of the expected dense error sequence $\{z_{\mu,k+1|k}\}_{k=0}^{\infty}$. We start by establishing the following fundamental lemmas, whose proofs are omitted due to space limitations.

Assumption 4: $\hat{\Gamma}_k$ has full column rank for all $k \in \mathbb{Z}_{\geq 0}$.

Assumption 4 ensures that $\hat{\Gamma}_k$ has an exact left pseudoinverse $\hat{\Gamma}_k^{\dagger}$ (i.e., $\hat{\Gamma}_k^{\dagger}\hat{\Gamma}_k = I_{n_\mu}$), but may also be interpreted as a condition on the excitation of the system. Specifically, $\hat{\Gamma}_k$ is rank-deficient if there exist columns with all zeros. Intuitively, this means that the forcing terms are "weakly" exciting, resulting in a lack of information regarding how each state changes with respect to an average. Such weak excitation makes recovering the exact change in each state challenging, and may even give rise to singularities. Thus, we impose the above assumption to avoid these issues.

Lemma 1: Under Assumption 4, the expected dense error dynamics of the coupled estimation scheme are

$$z_{\mu,k+1|k} = A_{\mu,k+1}(I_{n_\mu} - L_{\mu,k}H_{\mu,k})z_{\mu,k|k-1} + r_{\mu,k}, \quad (9)$$

where the additional error term $r_{\mu,k} := -A_{\mu,k+1}L_{\mu,k}\chi_\mu(z_{\mu,k|k-1})$ with $\chi_\mu(z_{\mu,k|k-1}) := \frac{1}{N}\chi(z_{k|k-1})$ accounts for measurement function nonlinearity.

Assumption 5: There exist real numbers $\overline{a_\mu}, \underline{a}, \overline{a}, \underline{\gamma}, \overline{\gamma}, \overline{h_\mu}, \underline{p_\mu}, \overline{p_\mu}, \underline{q_\mu}, \underline{r_\mu} \in \mathbb{R}_{>0}$ such that the following bounds are fulfilled for all $k \in \mathbb{Z}_{\geq 0}$: $\|A_{\mu,k}\| \leq \overline{a_\mu}$, $\underline{\gamma} \leq \left\|\hat{\Gamma}_k\right\| \leq \overline{\gamma}$, $\|H_{\mu,k}\| \leq \overline{h_\mu}$, $\underline{p_\mu}I_{n_\mu} \leq P_{\mu,k} \leq \overline{p_\mu}I_{n_\mu}$, $\underline{q_\mu}I_{n_\mu} \leq Q_{\mu,k}$, and $\underline{r_\mu} \leq R_{\mu,k}$.

We note that the bounds listed above are identical to those in the Kalman filter stability literature [8], but we add the upper and lower bounds on $\left\|\hat{\Gamma}_k\right\|$. For safety purposes, it is common in the battery control literature to impose box constraints on the current for each cell [9]. As shown in (6), $\hat{\Gamma}_k$ is directly dependent on the current of each cell, so it follows that there are also suitable bounds $\underline{\gamma}$ and $\overline{\gamma}$ that contain $\left\|\hat{\Gamma}_k\right\|$.

Lemma 2: Under Assumptions 1, 2, and 5, there exist constants $\epsilon', \kappa_{\text{nonl}} \in \mathbb{R}_{>0}$ such that $r_{\mu,k}^\top \Pi_{k+1}\left(2A_{\mu,k+1}(I_{n_\mu} - L_{\mu,k}H_{\mu,k})z_{\mu,k|k-1} + r_{\mu,k}\right) \leq \kappa_{\text{nonl}}\left\|z_{\mu,k|k-1}\right\|^3$ holds for $\left\|z_{\mu,k|k-1}\right\| \leq \epsilon'$, where $\Pi_k := P_{\mu,k+1|k}^{-1}$.

Lemma 3: Under Assumption 5, if we have the bound $\left\|z_{k|k-1}\right\| \leq \epsilon_\chi$ for some $\epsilon_\chi \in \mathbb{R}_{>0}$, then we also have the bound $\left\|z_{\mu,k|k-1}\right\| \leq \frac{\epsilon_\chi}{\underline{\gamma}}$.

Lemma 1 contains the expected dense error dynamics, with an affine term to account for the nonlinearity induced by the measurement function. Lemma 2 establishes an upper bound which comes in useful when proving Theorem 1 with Lyapunov functions, and Lemma 3 enables the easy conversion between bounds on the sparse error and bounds on the dense error. We now introduce the following theorem.

Theorem 1: Under Assumptions 1, 2, and 5, the expected dense error sequence $\{z_{\mu,k+1|k}\}_{k=0}^{\infty}$ is asymptotically stable provided that $\left\|z_{\mu,k|k-1}\right\| \leq \epsilon$ for all $k \in \mathbb{Z}_{\geq 0}$, where $0 < \epsilon < \min\left(\epsilon', \frac{\alpha}{\overline{p_\mu}\kappa_{\text{nonl}}}\right)$.

Proof: Consider the function $V(z_{\mu,k+1|k}) := z_{\mu,k+1|k}^\top P_{\mu,k+1|k}^{-1} z_{\mu,k+1|k}$, where Assumption 5 implies $P_{\mu,k+1|k} > 0$, making $V : \mathbb{R}^{n_\mu}\backslash\{0\} \mapsto \mathbb{R}_{>0}$ a suitable Lyapunov function. For brevity, we will abbreviate $V(z_{\mu,k+1|k})$ as V_{k+1}. Taking the difference of the Lyapunov function at two subsequent time steps, we have $V_{k+1} - V_k = z_{\mu,k+1|k}^\top P_{\mu,k+1|k}^{-1} z_{\mu,k+1|k} - z_{\mu,k|k-1}^\top P_{\mu,k|k-1}^{-1} z_{\mu,k|k-1}$. Substituting the result of Lemma 1 into the above yields

$$\begin{aligned}
&= \left[z_{\mu,k|k-1}^\top (I_{n_\mu} - L_{\mu,k}H_{\mu,k})^\top A_{\mu,k+1}^\top + r_{\mu,k}^\top\right] P_{\mu,k+1|k}^{-1} \\
&\quad \times \left[A_{\mu,k+1}(I_{n_\mu} - L_{\mu,k}H_{\mu,k})z_{\mu,k|k-1} + r_{\mu,k}\right] \\
&\quad - z_{\mu,k|k-1}^\top P_{\mu,k|k-1}^{-1} z_{\mu,k|k-1}, \\
&= z_{\mu,k|k-1}^\top (I_{n_\mu} - L_{\mu,k}H_{\mu,k})^\top A_{\mu,k+1}^\top P_{\mu,k+1|k}^{-1} \\
&\quad \times A_{\mu,k+1}(I_{n_\mu} - L_{\mu,k}H_{\mu,k})z_{\mu,k|k-1} + r_{\mu,k}^\top P_{\mu,k+1|k}^{-1} \\
&\quad \times \left[2A_{\mu,k+1}(I_{n_\mu} - L_{\mu,k}H_{\mu,k})z_{\mu,k|k-1} + r_{\mu,k}\right] \\
&\quad - z_{\mu,k|k-1}^\top P_{\mu,k|k-1}^{-1} z_{\mu,k|k-1}.
\end{aligned}$$

From here, we substitute the upper bound derived in Lemma 2 into the above and apply Assumption 5 to obtain

$$\begin{aligned}
&V_{k+1} - V_k \\
&\quad \leq z_{\mu,k|k-1}^\top (I_{n_\mu} - L_{\mu,k}H_{\mu,k})^\top A_{\mu,k+1}^\top P_{\mu,k+1|k}^{-1} \\
&\qquad \times A_{\mu,k+1}(I_{n_\mu} - L_{\mu,k}H_{\mu,k})z_{\mu,k|k-1} + \kappa_{\text{nonl}}\left\|z_{\mu,k|k-1}\right\|^3 \\
&\qquad - z_{\mu,k|k-1}^\top P_{\mu,k|k-1}^{-1} z_{\mu,k|k-1}, \\
&\quad \leq -\alpha V_k + \kappa_{\text{nonl}}\left\|z_{\mu,k|k-1}\right\|^3,
\end{aligned}$$

where $\alpha = 1 - \left(1 + \frac{\underline{q_\mu}}{\overline{p_\mu}(\overline{a_\mu} + \overline{a_\mu}\,\overline{p_\mu}\,\overline{h_\mu}^2/\underline{r_\mu})^2}\right)^{-1} \in \mathbb{R}_{(0,1)}$. Note that the result here is an upper bound on $V_{k+1} - V_k$ provided $\left\|z_{\mu,k|k-1}\right\| \leq \epsilon'$, where $\epsilon' > 0$. Furthermore, we may tighten the constraint to be $\left\|z_{\mu,k|k-1}\right\| < \epsilon$, where $\epsilon = \min\left(\epsilon', \frac{\alpha}{\overline{p_\mu}\kappa_{\text{nonl}}}\right) \leq \frac{\alpha}{\overline{p_\mu}\kappa_{\text{nonl}}}$. Applying ϵ to the upper bound, we have $-\alpha V_k + \kappa_{\text{nonl}}\left\|z_{\mu,k|k-1}\right\|^3 < -\alpha V_k + \kappa_{\text{nonl}}\epsilon\left\|z_{\mu,k|k-1}\right\|^2 \leq -\frac{\alpha}{\overline{p_\mu}}\left\|z_{\mu,k|k-1}\right\|^2 + \kappa_{\text{nonl}}\frac{\alpha}{\overline{p_\mu}\kappa_{\text{nonl}}}\left\|z_{\mu,k|k-1}\right\|^2 = 0$, confirming that the derived upper bound on $V_{k-1} - V_k$ is indeed negative, guaranteeing the strict decrease in the Lyapunov function for $\left\|z_{\mu,k|k-1}\right\| < \epsilon$. This completes the proof. ■

Remark 1: Because the above is a sketch proof of Theorem 1, we refer the reader to the proof of Theorem 3.1 put forth in [8] for a more detailed treatment – specifically, the derivation leading up to Equations (76) and (77) – which considers the equivalent scenario of extended Kalman filters that also abide by Assumptions 1, 2, and 5. In contrast to [8], we consider the expected error, which has the effect of removing all terms dependent on stochastic processes (i.e., $\mathbb{E}\left[2s_n^\top \Pi_{n+1}[(A_n - K_nC_n)\zeta_n + r_n] + s_n^\top \Pi_{n+1}s_n\right] = 0$).

B. Sparse Stability Analysis

This section is devoted to addressing the second half of Problem 1, which aims to ascertain the asymptotic behavior of $\{z_{k+1|k}\}_{k=0}^{\infty}$. First, Theorem 2 is introduced to confirm marginal stability in the absence of nonlinearity (i.e., $L = 0$). Afterwards, the case of nonlinearity ($L > 0$) is considered, for which a sufficient condition to maintain marginal stability is provided (Theorem 3). In a similar vein to Section IV-A, we introduce an additional set of lemmas which lay the groundwork for Theorems 2 and 3.

Lemma 4: Under Assumption 3, the expected sparse error dynamics propagated by the coupled DEKF estimation scheme are as follows:

$$z_{k+1|k} = \tilde{A}_{k+1}(I_{n_\mu N} - \tilde{L}_k\tilde{H}_k)z_{k|k-1} + r_k, \tag{12}$$

where $\tilde{A}_{k+1} := I_{n_\mu N} - \hat{\Gamma}_k\hat{\Gamma}_k^\dagger + \hat{\Gamma}_k\hat{\Gamma}_k^\dagger A_{k+1}\hat{\Gamma}_k\hat{\Gamma}_k^\dagger$, $\tilde{L}_k := \hat{\Gamma}_{k-1}L_{\mu,k}$, $\tilde{H}_k := H_{\mu,k}\hat{\Gamma}_{k-1}^\dagger$, and $r_k := -\frac{1}{N}\tilde{A}_{k+1}\tilde{L}_k\chi(z_{k|k-1})$.

Corollary 1: As a corollary to Lemma 4, we have that for a linear measurement function, $\chi(x_{k+1}, \hat{x}_{k+1}, u_k) = 0$. By Lemma 4, this implies $r_k = 0$, so we modify (12) accordingly to obtain the expected sparse error dynamics for linear measurement function $z_{k+1|k} = \tilde{A}_{k+1}(I_{n_\mu N} - \tilde{L}_k\tilde{H}_k)z_{k|k-1}$.

Lemma 5: Under Assumption 4, for a matrix $\Gamma \in \mathbb{R}^{m\times n}$ with $m \geq n$, Moore-Penrose pseudoinverse $\Gamma^\dagger \in \mathbb{R}^{n\times m}$, and a square matrix $G \in \mathbb{R}^{n\times n}$, we have $\Lambda(\Gamma G\Gamma^\dagger) = \Lambda(G) \cup \{0\}^{m-n}$.

Lemma 4 paired with Corollary 1 derives the dynamics of the expected sparse error dynamics for the cases of nonlinear and linear measurement functions, respectively. Additionally, the spectral properties of matrices made similar by a pseudoinverse are introduced in Lemma 5. To assess the sparse stability in the case of linear measurement function, this reduces to exploring the spectral properties of the modified error dynamics in Corollary 1. Therefore, we state the following theorem with the proof omitted due to space limitations.

Theorem 2: Under Assumptions 1, 2, 3, 4, and 5, for the case of a linear measurement function, i.e., $\chi(x_{k+1}, \hat{x}_{k+1|k}, u_k) = 0$, we have $\rho\left(\tilde{A}_{k+1}(I_{n_\mu N} - \tilde{L}_k\tilde{H}_k)\right) = 1$, i.e., the expected sparse error dynamics are marginally stable.

Recall the sparse expected error dynamics from Lemma 4, where the additional term r_k is due to the nonlinearity in the measurement function. While the effect of this added term on the spectrum of $\tilde{A}_{k+1}(I_{n_\mu N} - \tilde{L}_k\tilde{H}_k)$ is difficult to ascertain directly, we list the following theorem towards a sufficient condition for the asymptotic stability of (12) and emphasize its geometric intuition.

Theorem 3: The expected sparse error dynamics (12), with $L > 0$, are asymptotically stable if the projection coefficient $\frac{r_k^\top z_{k+1|k}}{\|r_k\|^2} < 1$ and $\|z_{k|k-1}\| \geq \|r_k\|$ for all $k \in \mathbb{Z}_{>0}$ (proof omitted due to space limitations).

Remark 2: We remark that the sufficient condition contained in Theorem 3 is geometrically intuitive. First, the condition $\|z_{k|k-1}\| \geq \|r_k\|$ constrains the size of the nonlinearity introduced to be smaller than the error present at any given time step. Second, the condition on the projection coefficient $\frac{r_k^\top z_{k+1|k}}{\|r_k\|^2} < 1$ ensures nonlinearity does not overly contribute to the error in the subsequent time step.

V. Simulation Results

A. Implementation Details

We implement the DEKF algorithm to simultaneously estimate SOC and open-circuit resistance R_o for $N = 3$ series-connected heterogeneous cells under constant load $u_k^i = 2$ A. Common parameters are $\eta = 0.9$, $C_{bat} = 5$ Ah, and $R_o = 1.34348 \times 10^{-2}$ Ω, with nominal values from [10] at 15°C. Heterogeneity is introduced by sampling (R_p^i, C_p^i) from $\mathcal{N}\big([\mu_R, \mu_C]^\top, \text{diag}\{\sigma_R^2, \sigma_C^2\}\big)$ with $\mu_R = 2.2166 \times 10^{-2}$, $\mu_C = 1.9974 \times 10^3$, and $\sigma = 0.01\mu$. OCV profiles use degree-10 polynomials fitted to data from [10]. Simulations run for 3600 s at $T_s = 1$ s with a lower saturation bound $R_{sat} = 10^{-3}$ on $\hat{R}_o^i$, using MATLAB R2024b on an Intel Core Ultra 7 155U.

B. Stable System

In pursuit of stable estimation, we take special care to initialize the DEKF algorithm and the system with appropriate values so that theoretical stability can be guaranteed apriori. To this end, we set $Q_{\mu,k} = \text{diag}\{10^{-10}, 10^{-10}, 10^{-10}\}$, $R_{\mu,k} = 10^{-4}$, $P_{\mu,0|0} = \text{diag}\{10^{-7}, 10^{-7}, 10^{-7}\}$, perturbations $\delta_i = 10^{-6}$, and initial estimates $\hat{x}_{0|0}^i = \begin{bmatrix}0.97 & 0 & 1.3\cdot 10^{-2}\end{bmatrix}^\top$ and $\hat{x}_{\mu,0|0} = \begin{bmatrix}0.97 & 0 & 1.3\cdot 10^{-2}\end{bmatrix}^\top$ for all $i \in \mathbb{Z}_{[1,N]}$ for the DEKF algorithm. For the simulation, we set process noise $w_{\mu,k} \in \mathcal{N}(0, Q_{\mu,k})$, measurement noise $v_k \sim \mathcal{N}(0, R_{\mu,k})$, and initial values $x_0^i = \begin{bmatrix}1 & 0 & 1.34348\cdot 10^{-2}\end{bmatrix}^\top$ and $x_{\mu,0} = \begin{bmatrix}1 & 0 & 1.34348\cdot 10^{-2}\end{bmatrix}^\top$. From this, we can establish the values of several of the constants introduced earlier in Assumptions 2 and 5. Namely, $\overline{a_\mu} = 1$, $\overline{a} = 1$, $\underline{q_\mu} = 10^{-10}$, $\underline{r_\mu} = 10^{-4}$. Furthermore, the OCV curves are processed offline along with preliminary simulations, which determine $\underline{\gamma} = 1.7320$, $\overline{\gamma} = 1.7321$, $\overline{h_\mu} = 8.0389$, $\underline{p_\mu} = 10^{-9}$, and $\overline{p_\mu} = 10^{-7}$ are adequate bounds on the corresponding matrices, and that $L = 1.28822\cdot 10^3$ appropriately characterizes the nonlinearity of the measurement function for $\epsilon_\chi = 0.1$. From here, we use the result in Theorem 1 to compute $\kappa' = 1.30797\cdot 10^{-4}$, $\kappa_{\text{nonl}} = 2.78502\cdot 10^5$, $\alpha = 8.81504\cdot 10^{-4}$, and the region of asymptotic stability $\epsilon = \min\left(\frac{\epsilon_\chi}{\underline{\gamma}}, \frac{\alpha}{\overline{p_\mu}\kappa_{\text{nonl}}}\right) = 4.74803\cdot 10^{-2}$. We compute $\|\zeta_{\mu,0|0}\| = \|\hat{x}_{\mu,0|0} - x_{\mu,0}\| = 3.00032\cdot 10^{-2} \leq \epsilon$. By this assessment, the expected dense error dynamics are guaranteed to be asymptotically stable per the result of Theorem 1.

The results of this simulation are shown in Fig. 1, where the SOC RMSE begins at $3\cdot 10^{-2}$ before leveling off at $7\cdot 10^{-3}$, while the parameter RMSE summits at a value of ≈ 0.0125 before rebounding at around $300 - 400$ seconds toward zero, indicating that the parameter estimates are converging. We note that the right-hand subplot in Fig. 1, per the theoretical findings, exhibits a spectral radius for the

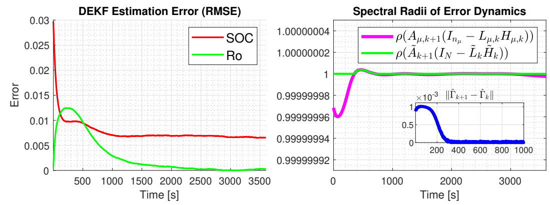

Fig. 1. Comparison of the stable SOC and parameter RMSE (left), spectral radii for the dense error dynamics (9) and sparse error dynamics (12) (right).

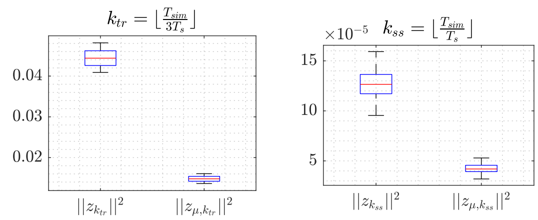

Fig. 2. Box-plot of stable sparse and dense errors during transient (left) and steady-state (right) collected over 100 simulations.

dense error dynamics less than or equal to 1 at all moments except for the transient period, where the error dynamics briefly become unstable. Recall one of the key assumptions (Assumption 3) that relies on constant values for $\hat{\Gamma}_k$. The superimposed plot indicates that this fundamental assumption is temporarily violated during the transient period, which is inevitable since $\hat{\Gamma}_k$ is a function of the estimates of each cell's relaxation voltage (6). Once voltage estimates stabilize, $\hat{\Gamma}_k$ stabilizes and the spectral radius remains in the stable region, confirming theoretical guarantees. Fig. 2 shows the average squared-error data over 100 trials at transient (1200 seconds) and steady-state (3600 seconds). As shown here, the transient interquartile ranges are 4.2-4.4×10^{-2} (sparse) and 1.4-1.6×10^{-2} (dense), while steady-state ranges are 1.15-1.35×10^{-4} (sparse) and 4-5×10^{-5} (dense), confirming the reduction of error, and consequently, the convergence of the DEKF estimation across numerous trials.

C. Noisy System

Finally, we investigate a practical scenario in which the initial estimates are far away from the true values and there is considerable noise present in the system. Specifically, we set $Q_{\mu,k} = \text{diag}\{10^{-7}, 10^{-7}, 10^{-9}\}$, $R_{\mu,k} = 5 \cdot 10^{-3}$, $P_{\mu,0|0} = \text{diag}\{10^{-2}, 10^{-4}, 10^{-4}\}$, perturbations $\delta_i = 10^{-6}$, and initial estimates $\hat{x}^i_{0|0} = \begin{bmatrix} 0.9 & 0 & 5 \cdot 10^{-2} \end{bmatrix}^\top$ and $\hat{x}_{\mu,0|0} = \begin{bmatrix} 0.9 & 0 & 5 \cdot 10^{-2} \end{bmatrix}^\top$ for all $i \in \mathbb{Z}_{[1,N]}$ for the DEKF algorithm. Furthermore, the process noise $w_{\mu,k} \in \mathcal{N}(0, Q_{\mu,k})$, measurement noise $v_k \sim \mathcal{N}(0, R_{\mu,k})$, and initial values $x^i_0 = \begin{bmatrix} 1 & 0 & 1.34348 \cdot 10^{-2} \end{bmatrix}^\top$ and $x_{\mu,0} = \begin{bmatrix} 1 & 0 & 1.34348 \cdot 10^{-2} \end{bmatrix}^\top$. Even in the presence of considerable measurement noise, the DEKF can still adhere quite well to the true SOC values, even if the initial estimates are inaccurate by ≈ 0.1. Specifically, Fig. 3 shows a sharp convergence of the parameter estimates towards their true values in the transient before settling to an RMSE

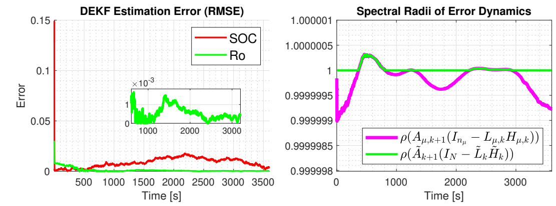

Fig. 3. Comparison of the noisy SOC and parameter RMSE (left), spectral radius of dense and sparse error dynamics (right).

of the order of 10^{-3} after approximately 700 seconds of the simulation have elapsed. Although the parameter error seems to dwindle, the SOC error shows no signs of a monotonic decrease over time. As can be seen, the SOC RMSE fluctuates between $0.01 - 0.02$ due to the error spectral radius regularly exceeding 1. This breach of the spectral radius occurs more frequently than in the other experiment (Fig. 3).

VI. Conclusion

This work modified the DEKF algorithm for simultaneous cell state-parameter estimation by injecting artificial perturbations into the dense model. We certified local asymptotic stability of the dense expected error under standard Kalman predictor assumptions, proved marginal stability of the sparse error without nonlinearity, and provided a sufficient condition for sparse asymptotic stability with nonlinearity via appropriate Lyapunov function selection. Simulation results with careful initialization, without noise, and with large noise verified the theoretical findings.

References

[1] Z. B. Omariba, L. Zhang, and D. Sun, "Review of battery cell balancing methodologies for optimizing battery pack performance in electric vehicles," *Ieee Access*, vol. 7, pp. 129 335–129 352, 2019.

[2] G. L. Plett, "Extended kalman filtering for battery management systems of lipb-based hev battery packs: Part 1. background," *Journal of Power Sources*, vol. 134, no. 2, pp. 252–261, 2004.

[3] F. Daum, "Nonlinear filters: beyond the kalman filter," *IEEE Aerospace and Electronic Systems Magazine*, vol. 20, no. 8, pp. 57–69, 2005.

[4] Z. Pei, X. Zhao, H. Yuan, Z. Peng, and L. Wu, "An equivalent circuit model for lithium battery of electric vehicle considering self-healing characteristic," *J. Control Sci. Eng.*, vol. 2018, 2018.

[5] H. He, R. Xiong, X. Zhang, F. Sun, and J. Fan, "State-of-charge estimation of the lithium-ion battery using an adaptive extended kalman filter based on an improved thevenin model," *IEEE Transactions on Vehicular Technology*, vol. 60, no. 4, pp. 1461–1469, 2011.

[6] L. Nuculaj and J. Chen, "Simultaneous cell state estimation via dense adaptive extended kalman filter," *IEEE Transactions on Control Systems Technology*, 2025, to appear.

[7] E. Blanchard, A. Sandu, and C. Sandu, "Parameter estimation method using an extended kalman filter," 2007.

[8] K. Reif, S. Gunther, E. Yaz, and R. Unbehauen, "Stochastic stability of the discrete-time extended Kalman filter," *IEEE Transactions on Automatic control*, vol. 44, no. 4, pp. 714–728, 1999.

[9] J. Chen, A. Behal, Z. Li, and C. Li, "Active battery cell balancing by real time model predictive control for extending electric vehicle driving range," *IEEE Trans. Auto. Sci. Eng.*, vol. 21, no. 3, pp. 4003–4015, July 2024.

[10] X. Lin, H. E. Perez, J. B. Siegel, A. G. Stefanopoulou, Y. Li, R. D. Anderson, Y. Ding, and M. P. Castanier, "Online parameterization of lumped thermal dynamics in cylindrical lithium ion batteries for core temperature estimation and health monitoring," *IEEE Transactions on Control Systems Technology*, vol. 21, no. 5, pp. 1745–1755, 2012.